Dispersion-Based Fresh-Slice Scheme for Free-Electron Lasers

Marc W. Guetg,* Alberto A. Lutman, Yuantao Ding, Timothy J. Maxwell, and Zhirong Huang
SLAC National Accelerator Laboratory, Menlo Park, California 94025, USA

(Received 6 March 2018; published 28 June 2018)

The fresh-slice technique improved the performance of several self-amplified spontaneous emission free-electron laser schemes by granting selective control on the temporal lasing slice without spoiling the other electron bunch slices. So far, the implementation has required a special insertion device to create the beam yaw, called a dechirper. We demonstrate a novel scheme to enable fresh-slice operation based on electron energy chirp and orbit dispersion that can be implemented at any free-electron laser facility without additional hardware.

DOI: 10.1103/PhysRevLett.120.264802

X-ray free-electron lasers (XFEL) are the brightest x-ray light sources for scientific applications [1,2]. With their high-intensity photon pulses, XFELs have been used in a broad range of scientific experiments in the physical [3], chemical [4], life [5], and material sciences [6]. X-ray FEL machines were initially designed to produce a single x-ray pulse with a duration ranging from tens to hundreds of femtoseconds. Recently, in an effort to satisfy the requirements of the wide scientific community, FEL x-ray shaping has been an active field of investigation. Ultrashort pulses are produced to exploit the probe-before-destroy principle for single-particle imaging [7,8] and femtosecond x-ray crystallography [9] with an array of techniques [10–15]. Few-femtosecond intense pulses can be produced with multistage fresh-slice amplification [16] and are suitable for creating double core-hole states [17] and to reveal a variety of nonlinear phenomena when intense x-ray pulses interact with atoms and molecules [3,18], including stimulated emission [19]. X-ray pump, x-ray probe experiments (see, for example, Refs. [20,21]) were enabled by double-pulse schemes [22–26]. Narrow bandwidth and spectral stability granted by the self-seeding schemes [27,28] were used to study the dynamics of warm dense matter systems [29] and for x-ray absorption spectroscopy [30].

The recent demonstration of the fresh-slice [26] technique enabled or improved the performance of many aforementioned schemes. The fresh-slice scheme grants control over the temporal slice lasing in each undulator section by manipulating the orbits of individual slices. A device imparts a time-dependent kick to the electrons, causing the bunch slices to travel on monotonically increasing oscillating trajectories in the strong focusing lattice. In an undulator section, the sustained coherent interaction between a microbunched beam and the electromagnetic field is not preserved for a large oscillatory orbit [10,31], and therefore the lasing slice can be selected as the one traveling on a straight orbit.

Unlike other techniques [11–13], the lasing-suppressed slices retain full lasing capability to be exploited in downstream undulator sections. In two-color modes, higher power and enhanced pulse customizability were demonstrated. Three fully saturated x-ray pulses of different colors were produced for the first time. High-power single-coherent spikes were demonstrated in a multistage scheme [16], and by using additional cascaded amplification stages, terawatt powers could be reached [32]. Combined with self-seeding, the fresh-slice technique improved the achievable power in the hard x rays [33]. It is planned to be used for harmonic lasing at the Linac Coherent Light Source (LCLS) [34] and to produce double sub-femtosecond pulses [35].

The fresh-slice technique has been demonstrated by tailoring the electron bunch with a temporal-transverse correlation and subsequent fine bunch orbit control in the undulator line. Alternatively, a scheme based on time-dependent matching rather than orbit has been proposed [36,37], which exploits the transverse focusing term of the dechirper [37]. At the LCLS, the temporal-transverse correlation is imparted by the strong transverse wakefield of a dechirper [38–40], providing sufficient beam yaw for the lasing suppression. Alternatively, a quadrupole magnet in a dispersive area and transverse deflecting cavities were also proposed to induce the required beam yaw [31,41,42].

This Letter describes the first demonstration of a fresh-slice scheme based on electron energy chirp and orbit dispersion. In contrast to other fresh-slice implementations, the presented one does not require any special insertion device and therefore can be used at any existing XFEL facility without the installation of additional hardware. Dispersion-based fresh slice represents a viable solution for future high-repetition-rate machines where dechirper-based schemes may suffer from the violation of beam stay-clear requirements [43] and excessive heating on the dechirper jaws. Furthermore, provided a linearly energy-chirped electron bunch in the dispersive area, the induced beam yaw is linear, granting more uniform pulse durations in double-pulse modes. This pulse length uniformity is

important for nonlinear two-photon two-color interactions, as the shorter pulse limits the overlap. Furthermore, the longer pulse limits the temporal resolution for any x-ray-pump y-ray-probe and x-ray-probe x-ray-probe experiments, therefore making it more suited for this experiment than the dechirper-based fresh-slice scheme.

Similar to the dechirper-based method, the dispersion one does not suffer from beam arrival time to radio-frequency phase jitter, which is a limitation of the radio-frequency transverse deflecting cavity implementation. Finally, the presented scheme stabilizes FEL radiation wavelength, granting an advantage over competing schemes when generating a single short pulse from a long electron bunch. This could lead to improved usage of stochastic stimulated x-ray Raman spectroscopy [44] and easier data sorting for serial femtosecond crystallography [45]. Furthermore, the energy stabilization could also lead to improved fresh-slice self-seeding performance, as the bandwidth stability is believed to be one of the limiting factors.

In the dispersion-based fresh-slice scheme presented here, the beam yaw required to select lasing slices is created by controlling the dispersion in a beam with large energy chirp. Figure 1(a) illustrates a schematic drawing of the LCLS with parts relevant to the demonstrated scheme. The electron bunch is accelerated in the linac sections (orange) and compressed in two bunch compressors (BCs). Overcompressing the electron bunch within the last BC flips the sign of the energy chirp. The longitudinal wakefields of the third section of the linac further increase the energy chirp when operating in overcompression mode allowing one to generate energy chirps well above 1%, the size commonly used for large-bandwidth lasing. The overcompressed bunch then traverses a dispersive dogleg section with two dispersion tweaker quadrupoles to manipulate the dispersion. In a dispersive section, particles with different longitudinal momentum travel on different transverse orbits. When passing the quadrupoles, the electrons receive a transverse kick depending on their transverse trajectory. For an electron bunch with an energy chirp traveling through a dispersive section, this is a means to introduce a time-dependent kick, which then translates into a beam yaw through betatronic phase advance. The amount of beam yaw can be controlled by increasing either the energy chirp or the dispersion.

LCLS is equipped with a pair of quadrupole magnets to finely control dispersion in amplitude and phase in both bunch compressors and the final dogleg. Alternatively, the dispersion is controlled by orbit bumps after the final dogleg. Hereby the dispersion is manipulated by the introduction of an orbit offset within strong quadrupole magnets. This method has the added benefit of not altering transverse matching and therefore not requiring rematching.

Finally, the bunch enters the undulator line, which is split into three sections separated by magnetic chicanes introduced for self-seeding schemes [27,28,46]. In addition, there is a pair of orthogonal orbit correctors between each undulator segment to control the orbit position and angle. Only electrons traveling on axis through the undulator contribute to lasing, so selection of the lasing slice is done by setting a proper electron bunch orbit in the undulator line [Fig. 1(b)]. Steering the orbit within the undulator line enables the selection of different lasing slices for different sections [Fig. 1(c)].

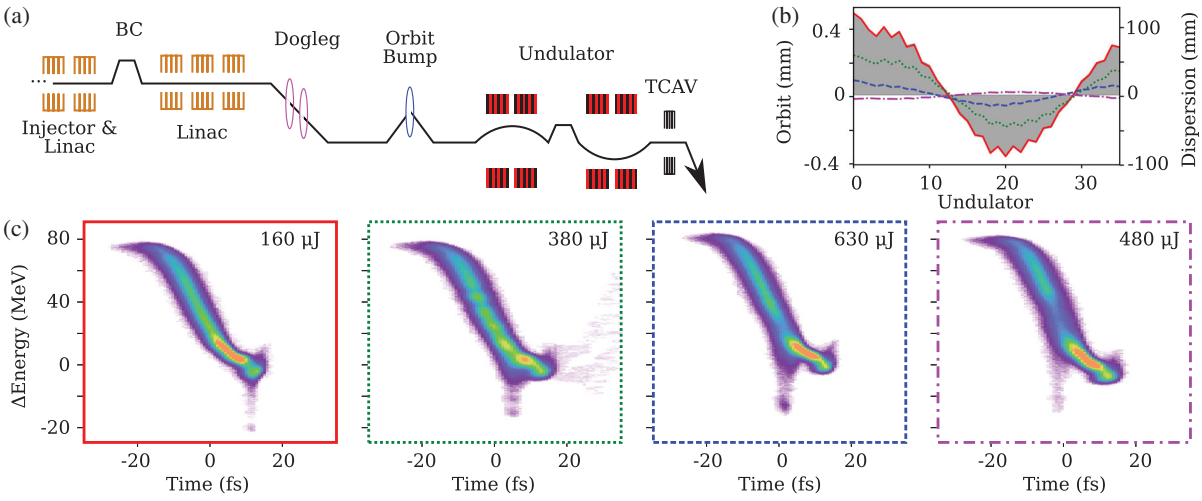

FIG. 1. (a) Schematic experimental setup for the LCLS. The electrons coming from the linac (left) are overcompressed in the last bunch compressor, followed by the last linac section adding both energy and chirp, which is followed by the dogleg, containing two tweaker quadrupole magnets (magenta) to control dispersion, followed by an orbit bump (blue) and the undulators (red and black). A transverse deflector following spectrometer allows direct longitudinal phase space measurements. (b) Dispersion (filled, gray) within the undulator with four different selected orbits leading to selective lasing within the electron beams shown in (c). Electron beam energy: 10.1 GeV, charge: 185 pC.

Since different slices have different electron energies, they lase at different colors, so two-color double pulses with a wide range of color separation can be produced by changing the orbit between undulator sections. The time difference between the photon pulses is mainly controlled by a magnetic chicane located between the undulator sections, which delays the arrival of the lasing electron slice in the downstream undulator section with respect to the upstream generated photon pulse [see also Fig. 4(a)]. When a slice on the bunch tail is used to produce the x-ray pulse in the upstream undulator section, then the delay between the pulses can be scanned smoothly through the time coincidence. Instead, if the pulse produced in the upstream undulator section is on the bunch head, there is a minimum delay of ten to a few tens of femtoseconds between the two pulses. Thus, if pulse overlap or scanning in the first few femtoseconds of the delay range is required for an experiment, then the possible photon energy range at LCLS is asymmetric, with the pulse produced from the bunch tail (pump) ranging from the same wavelength to −4% compared to the pulse produced from the bunch head (probe).

Inherent to the dispersion-based fresh-slice scheme is a stable FEL radiation wavelength, which is not affected by the electron bunch energy jitter as long as the jitter is smaller than the unsuppressed FEL bandwidth, which is normally given—for this specific experiment, by more than 1 order of magnitude. For a Self Amplified Spontaneous Emission (SASE) FEL, the radiated photon energy is proportional to the square of the electron energy, leading to a relative photon energy jitter twice the relative electron energy jitter. Using the dispersion-based fresh-slice scheme, the lasing slice is selected as the one traveling on a straight line in the undulator line, which corresponds to an electron bunch slice with defined energy. Therefore, the electron bunch shot-to-shot energy jitter causes a jitter in the position of the lasing slice instead of a radiation wavelength jitter. This is a valuable feature unique to the presented method. For instance, in the dechirper-based fresh-slice, the lasing slice is selected as a bunch slice having a defined temporal coordinate within the bunch [26], and the lasing wavelength is thus sensitive to electron energy jitter. For a slotted-foil pulse duration control scheme [12], energy selection occurs in the second bunch compressor, but energy jitter can still be added in the third linac section and thus influence radiation wavelength.

The demonstration of selective lasing control was performed at the LCLS in overcompression mode for several energies. The electron bunch was operated at a nominal charge of 250 pC at the injector and collimated to 180 pC at the first bunch compressor [47]. For soft x rays, the electron bunch energy was 5680 ± 3.1 (rms) MeV, and a photon energy jitter of 0.08% was measured.

For the experiments presented in this Letter, the undulator orbit was set by manipulating multiple correctors in the undulator line, and just upstream from the undulator line. The target orbit was chosen by scaling the orbit recorded after a perturbation of the tweaker quadrupole magnet with the transverse orbit feedbacks turned off. The amount of scaling required for lasing on a particular slice was determined empirically by observing the lasing footprint of the time-resolved electron bunch phase space downstream of the undulator line.

Comparing the time-resolved electron bunch energy spaces downstream of the undulator line [Figs. 2(a) and 2(b)] reveals that both setups have the same amount of electron energy loss, which indicates that FEL power was not altered by the fresh-slice scheme. The x-ray power temporal profile [Figs. 2(c) and 2(d)] was measured by analyzing the time-resolved electron phase space lasing-on footprints compared to the lasing-off ones [48]. The FEL process both increases the slice energy spread and decreases the slice centroid energy. The temporal profile of the photon pulse was estimated independently with both of the quantities.

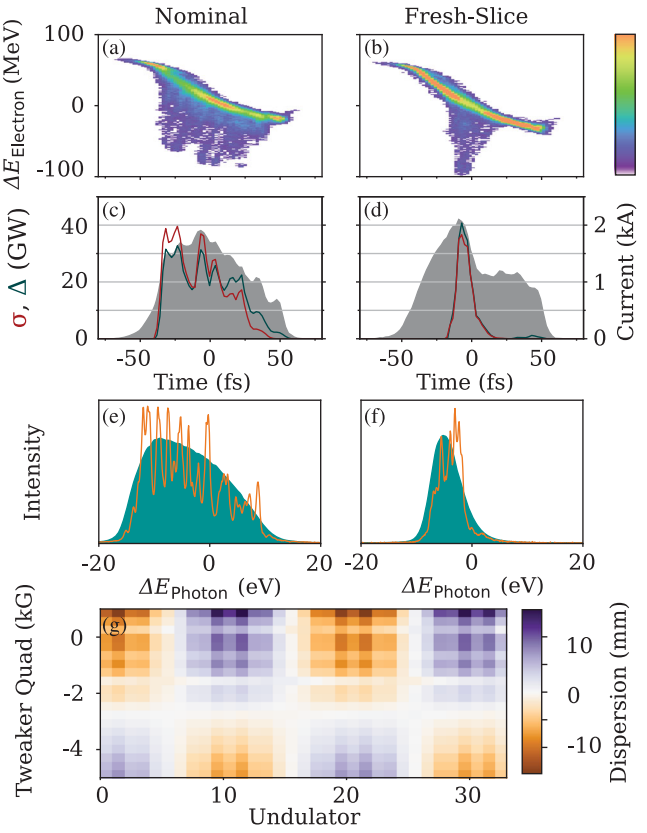

FIG. 2. Left: Uniform lasing. Right: Fresh-slice lasing. (a,b) Longitudinal electron phase space after the undulator. (c,d) Photon power calculated by energy loss (Δ, green) and slice energy spread (σ, red) overlaid over the current profile (grey). (e,f) Single-shot (brown) and average (cyan) photon spectrum. (g) Dispersion within the undulator created by scanning the second tweaker quadrupole magnet within the dog leg. Electron charge 180 pC, electron energy 5.68 GeV, mean photon energy 1.5 keV.

The measurement based on the energy spread increase (in red) agrees well with the one based on the slice energy losses (in blue). These measurements show how the x-ray pulse duration is reduced through the fresh-slice scheme. Comparing single-shot or average spectra for each setup [Figs. 2(e) and 2(f)] as measured at the soft x-ray experimental station with a grating spectrometer [49,50] shows that the fresh-slice scheme also narrows the spectral width of the x-ray pulse. Figure 2(g) shows the dispersion within the undulator by scanning a tweaker quadrupole within the dogleg. Together with the energy chirp, this is a measurement of the off-axis oscillation amplitude of individual slices.

To further investigate the spectral stability of the scheme, we compared the setup in standard overcompression mode (low dispersion) to fresh-slice mode (high dispersion). Figure 3(a) displays the ratio between photon energy jitter and electron bunch energy jitter as a function of the dispersion in Genesis [51] simulations and measurements. It shows that for large absolute dispersion values, corresponding to fresh-slice mode, the photon wavelength is stable, while there is no wavelength stabilization for low dispersion values. Next, two experimental operating points were considered, one with minimal dispersion and one with large dispersion [Fig. 3(b)]. Comparing the average photon spectra as functions of electron bunch energy shows a stable wavelength and narrow bandwidth for large dispersion, while at low dispersion the wavelength is energy dependent and the spectral bandwidth is wide.

Looking at the electron orbit position within the undulator line for shots at higher or lower than target electron energy [Fig. 3(e)], we observe that the orbit shifts in high-dispersion mode, while it remains constant for the low-dispersion mode. This orbit shift inherent to the fresh-slice mode results in selection of a different lasing slice and thereby corrects for the offset in electron bunch energy, leading to the observed spectral stability.

To further explore the capabilities of the method, a two-color scheme with dispersion-based fresh slice was developed. A first color was produced on the bunch core in the first undulator section, before the second chicane of the LCLS undulator line. Downstream of the chicane, the orbit was manipulated to lase on a slice toward the bunch tail. We repeated the experiment for two different slices on the bunch tail while keeping the first color constant. Figure 4(a) shows the position of the bunch orbit center of mass throughout the undulator. In the first undulator section,

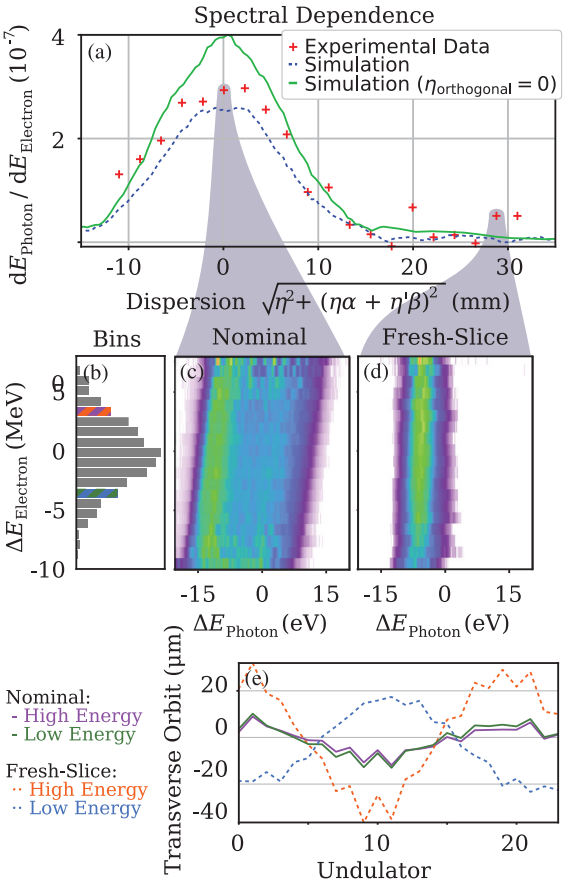

FIG. 3. (a) Spectral stability of the photon beam for measurement (red), Genesis [51] simulation of it (blue), and an idealized case (green) without dispersion in the dimension orthogonal to the measurement plane. (c,d) Spectral measurements of two dispersion settings (marked grey area). The spectra are averaged and binned by electron energy. (b) Histogram showing the energy distribution of the measured pulses. (e) The averaged electron orbits for one high and one low energy bin (marked in histogram at middle and left). For the low-dispersion case, both orbits are on top of each other. Electron energy: 5.68 GeV, photon energy: 1.5 keV. The electron beam was kicked after undulator 25 to preserve suppression.

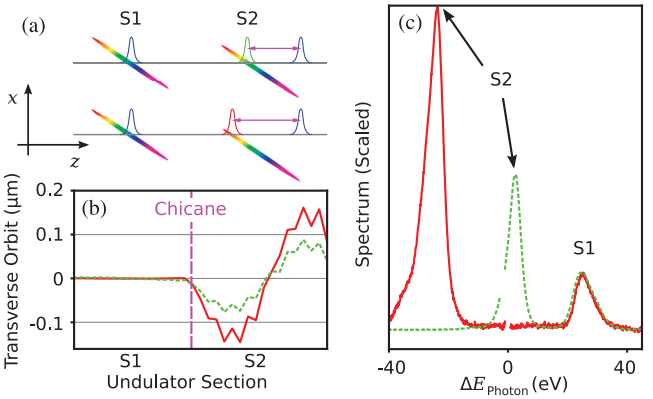

FIG. 4. (a) Schematic drawing of two-color operation with lasing in two locations of the same electron bunch. (b) Two measured electron orbits selecting a common first color and an individual second. The delay between the pulses is controlled by a self-seeding chicane (magenta). (c) Average spectrum of both cases. The missing spectral data are due to a broken YAG scintillator. Mean photon energy: 1.5 keV, with individual shots of over 100 μJ (average 20 μJ) with a color separation of more than 4%.

the lasing slice is on the bunch core, so the orbit does not oscillate, while in the second undulator section the lasing slice is distant from the bunch core, which is visible by the oscillation of the orbit. Selecting a lasing slice closer to the bunch core (green) requires an orbit with lower oscillation amplitude, while a lasing slice more distant from the core (red) needs higher amplitude. Using the slice closer to the bunch core (blue) resulted in an energy separation between the two colors of ~30 eV [Fig. 4(b), green] while using the slice more distant to the core (red) produced x rays with a separation of ~60 eV. This corresponds to a relative energy separation of 4%, which is the widest relative color separation of photon pulses at LCLS observed in any two-color mode so far.

The temporal delay between the photon pulses initially depends on the temporal distance between the selected lasing slices and slippage, but it can be adjusted by a time delay introduced at the magnetic chicane located between undulator sections. Therefore, the temporal delay between pulses is virtually independent of the chosen pulse colors.

In machines with variable gap undulators, each pulse wavelength can be independently adjusted in a wide range by the strength K of the undulators [23]. However, the LCLS K range is already sufficient to tune the different slices at the same wavelength, thereby enabling the multistage amplification schemes [16]. Controlling the dispersion within the second bunch compressor is an alternative method to produce a tilted beam without using the overcompression mode or additional hardware. However, transporting such a beam from the bunch compressor to the undulator line can degrade the electron bunch quality for slices traveling off axis, and the energy stabilization would no longer be superior to the one provided by the slotted foil. In summary, we demonstrated a dispersion-based fresh-slice scheme readily available at any XFEL facility without additional hardware. Control of the required dispersion, energy chirp, and orbit are simple to implement, and the scheme offers improved spectral stability. The latter feature is valuable for experiments requiring wavelength stability in a short pulse and multistage self-seeding schemes [33].

This work has been supported by DOE Contract No. DE-AC02-76SF00515. The authors thank the operators of LCLS for their excellent handling of the machine and Sandra Guetg for proofreading the manuscript. Furthermore, the authors thank Uwe Bergmann for fruitful discussions.

*marcg@slac.stanford.edu

[1] P. Emma *et al.*, Nat. Photonics **4**, 641 (2010).
[2] T. Ishikawa *et al.*, Nat. Photonics **6**, 540 (2012).
[3] Young *et al.*, Nature (London) **466**, 56 (2010).
[4] W. Zhang *et al.*, Nature (London) **509**, 345 (2014).
[5] H. N. Chapman *et al.*, Nature (London) **470**, 73 (2011).
[6] D. Milathianaki *et al.*, Science **342**, 220 (2013), http://science.sciencemag.org/content/342/6155/220.full.pdf.
[7] M. Seibert *et al.*, Nature (London) **470**, 78 (2011).
[8] A. Aquila *et al.*, Struct. Dyn. **2**, 041701 (2015).
[9] H. N. Chapman, C. Caleman, and N. Timneanu, Phil. Trans. R. Soc. B **369**, 20130313 (2014).
[10] M. W. Guetg, A. A. Lutman, Y. Ding, T. J. Maxwell, F.-J. Decker, U. Bergmann, and Z. Huang, Phys. Rev. Lett. **120**, 014801 (2018).
[11] P. Emma, K. Bane, M. Cornacchia, Z. Huang, H. Schlarb, G. Stupakov, and D. Walz, Phys. Rev. Lett. **92**, 074801 (2004).
[12] Y. Ding *et al.*, Appl. Phys. Lett. **107**, 191104 (2015).
[13] A. Marinelli, R. Coffee, S. Vetter, P. Hering, G. N. West, S. Gilevich, A. A. Lutman, S. Li, T. Maxwell, J. Galayda, A. Fry, and Z. Huang, Phys. Rev. Lett. **116**, 254801 (2016).
[14] S. Huang, Y. Ding, Y. Feng, E. Hemsing, Z. Huang, J. Krzywinski, A. A. Lutman, A. Marinelli, T. J. Maxwell, and D. Zhu, Phys. Rev. Lett. **119**, 154801 (2017).
[15] A. Marinelli, J. MacArthur, P. Emma, M. Guetg, C. Field, D. Kharakh, A. A. Lutman, Y. Ding, and Z. Huang, Appl. Phys. Lett. **111**, 151101 (2017).
[16] A. A. Lutman, M. Guetg, T. J. Maxwell, J. P. MacArthur, Y. Ding, C. Emma, J. Krzywinski, A. Marinelli, and Z. Huang, Phys. Rev. Lett. **120**, 264801 (2018).
[17] N. Berrah *et al.*, Proc. Natl. Acad. Sci. U.S.A. **108**, 16912 (2011), http://www.pnas.org/content/108/41/16912.full.pdf.
[18] J. Stöhr and A. Scherz, Phys. Rev. Lett. **115**, 107402 (2015).
[19] T. Kroll *et al.*, Phys. Rev. Lett. **120**, 133203 (2018).
[20] K. R. Ferguson *et al.*, Sci. Adv. **2**, e1500837 (2016).
[21] A. Picón *et al.*, Nat. Commun. **7**, 11652 (2016).
[22] A. A. Lutman, R. Coffee, Y. Ding, Z. Huang, J. Krzywinski, T. Maxwell, M. Messerschmidt, and H.-D. Nuhn, Phys. Rev. Lett. **110**, 134801 (2013).
[23] T. Hara *et al.*, Nat. Commun. **4**, 2919 (2013).
[24] A. Marinelli, A. A. Lutman, J. Wu, Y. Ding, J. Krzywinski, H.-D. Nuhn, Y. Feng, R. N. Coffee, and C. Pellegrini, Phys. Rev. Lett. **111**, 134801 (2013).
[25] A. Marinelli *et al.*, Nat. Commun. **6**, 6369 (2015).
[26] A. A. Lutman, T. J. Maxwell, J. P. MacArthur, M. W. Guetg, N. Berrah, R. N. Coffee, Y. Ding, Z. Huang, A. Marinelli, S. Moeller, and J. C. U. Zemella, Nat. Photonics **10**, 745 (2016).
[27] A. A. Lutman *et al.*, Phys. Rev. Lett. **113**, 254801 (2014).
[28] D. Ratner *et al.*, Phys. Rev. Lett. **114**, 054801 (2015).
[29] L. B. Fletcher *et al.*, Nat. Photonics **9**, 274 (2015).
[30] T. Kroll *et al.*, Opt. Express **24**, 22469 (2016).
[31] M. W. Guetg, B. Beutner, and E. P. S. Reiche, Phys. Rev. ST Accel. Beams **18**, 030701 (2015).
[32] E. Prat, F. Löhl, and S. Reiche, Phys. Rev. ST Accel. Beams **18**, 100701 (2015).
[33] C. Emma, A. Lutman, M. W. Guetg, J. Krzywinski, A. Marinelli, J. Wu, and C. Pellegrini, Appl. Phys. Lett. **110**, 154101 (2017).
[34] C. Emma, Y. Feng, D. C. Nguyen, A. Ratti, and C. Pellegrini, Phys. Rev. Accel. Beams **20**, 030701 (2017).
[35] J. MacArthur, J. Duris, Z. Huang, and A. Marinelli, in *8th International Particle Accelerator Conf. (IPAC'17), Copenhagen, Denmark, 2017* (JACOW, Geneva, Switzerland, 2017), pp. 2848–2850.
[36] Y.-C. Chao, Technical Report SLAC-PUB-16935, 2017.

[37] W. Qin, Y. Ding, A. A. Lutman, and Y.-C. Chao, Phys. Rev. Accel. Beams **20**, 090701 (2017).
[38] K. Bane and G. Stupakov, Nucl. Instrum. Methods Phys. Res., Sect. A **690**, 106 (2012).
[39] J. Zemella, K. Bane, A. Fisher, M. Guetg, Z. Huang, R. Iverson, P. Krejcik, A. Lutman, T. Maxwell, A. Novokhatski, G. Stupakov, Z. Zhang, M. Harrison, and M. Ruelas, Phys. Rev. Accel. Beams **20**, 104403 (2017).
[40] M. Guetg *et al.*, in *Proceedings of the International Particle Accelerator Conference (IPAC'16), Busan, Korea, 2016*, (JACoW, Geneva, Switzerland, 2016), pp. 809–812, http://accelconf.web.cern.ch/AccelConf/ipac2016/papers/mopow044.pdf.
[41] E. Prat, S. Bettoni, and S. Reiche, Nucl. Instrum. Methods Phys. Res., Sect. A **865**, 1 (2017).
[42] M. W. Guetg, Ph. D. thesis, ETH Zurich, 2015.
[43] P. Emma, LCLS Technical Report No. LCLS-II-2.1-PR-0352, 2015.
[44] V. Kimberg and N. Rohringer, Struct. Dyn. **3**, 034101 (2016).
[45] A. Meents *et al.*, Nat. Commun. **8**, 1281 (2017).
[46] J. Amman *et al.*, Nat. Photonics **6**, 693 (2012).
[47] Y. Ding *et al.*, Phys. Rev. Accel. Beams **19**, 100703 (2016).
[48] C. Behrens *et al.*, Nat. Commun. **5**, 3762 (2014).
[49] P. Heimann *et al.*, Rev. Sci. Instrum. **82**, 093104 (2011).
[50] J. J. Turner *et al.*, J. Synchrotron Radiat. **22**, 621 (2015).
[51] S. Reiche, Nucl. Instrum. Methods Phys. Res., Sect. A **429**, 243 (1999).